The Astrophysical Journal Letters, 740:L46 (6pp), 2011 October 20 doi:10.1088/2041-8205/740/2/L46

FREQUENCY FILTERING OF TORSIONAL ALFVÉN WAVES BY CHROMOSPHERIC MAGNETIC FIELD

V. Fedun[1], G. Verth[2], D. B. Jess[3], and R. Erdélyi[1]
[1] School of Mathematics and Statistics, University of Sheffield, Hounsfield Road, Hicks Building, Sheffield S3 7RH, UK
[2] School of Computing, Engineering & Information Sciences, Northumbria University, Newcastle Upon Tyne NE1 8ST, UK
[3] Astrophysics Research Centre, School of Mathematics and Physics, Queen's University, Belfast University Road, Belfast BT7 1NN, UK
Received 2011 June 21; accepted 2011 August 5; published 2011 September 30

ABSTRACT

In this Letter, we demonstrate how the observation of broadband frequency propagating torsional Alfvén waves in chromospheric magnetic flux tubes can provide valuable insight into their magnetic field structure. By implementing a full nonlinear three-dimensional magnetohydrodynamic numerical simulation with a realistic vortex driver, we demonstrate how the plasma structure of chromospheric magnetic flux tubes can act as a spatially dependent frequency filter for torsional Alfvén waves. Importantly, for solar magnetoseismology applications, this frequency filtering is found to be strongly dependent on magnetic field structure. With reference to an observational case study of propagating torsional Alfvén waves using spectroscopic data from the Swedish Solar Telescope, we demonstrate how the observed two-dimensional spatial distribution of maximum power Fourier frequency shows a strong correlation with our forward model. This opens the possibility of beginning an era of chromospheric magnetoseismology, to complement the more traditional methods of mapping the magnetic field structure of the solar chromosphere.

Key words: magnetic fields – magnetohydrodynamics (MHD) – Sun: atmosphere – Sun: chromosphere – Sun: photosphere

Online-only material: color figures

1. INTRODUCTION

It is now widely believed that plasma heating in the solar atmosphere, both at chromospheric and coronal heights, is due to physical processes driven by the Sun's magnetic field (see, e.g., Taroyan & Erdélyi 2009 for a recent review). However, the exact nature of the process (or processes) involved is still a cause for debate both from a theoretical and observational point of view. Regarding the observational aspects, direct measurement of the Sun's magnetic field above photospheric heights presents the most problems. It is crucial that progress is made in this area, so that we can quantify the magnetic energy available for plasma heating. One approach is only to use photospheric magnetogram data and extrapolate the magnetic field to higher altitudes, assuming potential or force-free conditions. Metcalf et al. (1995) estimate that the chromosphere is not force-free at heights less than 400 km, thereby questioning the validity of the lower boundary conditions of such calculations.

Regarding direct measurements at chromospheric heights, there have been attempts to measure the Zeeman (for stronger fields $\approx$ 1000 G) and Hanle effect (for weaker fields in the sub-Gauss to tens of Gauss regime) using the He I 10830 Å triplet (formed near the coronal base; see Lagg 2007 for a review of this topic). The poor signal-to-noise ratio of this type of measurement requires large integration times. For example, Centeno et al. (2010) attempted to measure the magnetic field strength of spicules in the chromosphere with an integration time of 45 minutes. Since spicules have a relatively short lifetime of 5–15 minutes (Zaqarashvili & Erdélyi 2009), spectropolarimetric measurements of this kind cannot estimate magnetic field strength of spicules within their lifetime. A vector polarimetry technique also using He I multiplet proposed by Solanki et al. (2003) to produce three-dimensional (3D) magnetic maps of the chromosphere has been debated by Judge (2009), since it was found to give spurious results for simple test cases.

Theoretically, it has been proposed that chromospheric flux tubes must undergo large expansion above the photosphere, the so-called magnetic canopy effect, e.g., Gabriel (1976). So far, using simultaneous photospheric and chromospheric magnetograms, evidence of this expansion has not been found directly (see, e.g., Zhang & Zhang 2000). Alternative indirect approaches have been attempted by, e.g., Kontar et al. (2008) to estimate the expansion in the chromospheric region of a flaring loop using *Reuven Ramaty High Energy Solar Spectroscopic Imager* (*RHESSI*) hard X-ray data, however, this technique had the largest uncertainty at heights less than 400 km. This indirect technique, therefore, can shed no further light on the conclusions by Metcalf et al. (1995). More recently, with spectropolarimeter data from the Solar Optical Telescope (SOT) aboard *Hinode*, Tsuneta et al. (2008) estimated an upper limit area expansion for flux tubes between the photosphere and corona in the southern polar region of the Sun to be about 345.

To complement these traditional methods of understanding the structure of the chromospheric magnetic field, the technique of magnetoseismology can also be implemented (see Banerjee et al. 2007 for a review of this topic). Thanks to modern high spatial/temporal resolution instrumentation a wide variety of propagating magnetohydrodynamic (MHD) wave modes have now been identified in the lower solar atmosphere, e.g., sausage (Morton et al. 2011), kink (He et al. 2009), and torsional Alfvén (Jess et al. 2009). By studying the observables of these MHD wave modes as a function of height this can give valuable insight into the structure of different chromospheric waveguides (e.g., magnetic pores, magnetic bright points, and spicules).

Often generated waves exhibit only one dominant frequency, e.g., in spicule kink waves. A recent example of a kink wave propagating with a dominant frequency in a spicule, which was

exploited for magnetoseismology, was Verth et al. (2011). They used the high spatial/temporal resolution of SOT to determine the vertical gradient in both magnetic field and plasma density in a spicule by studying the change in velocity and phase speed with height. If a broadband frequency of propagating waves can be detected in a solar waveguide, this offers richer possibilities for solar magnetoseismology. From observations, using the Coronal Multi-Channel Polarimeter (CoMP), it has been shown that broadband frequency kink waves exhibit a frequency-dependent damping length due to a perpendicular (to the magnetic field direction) gradient in the equilibrium Alfvén speed (Verth et al. 2010b), through the process of resonant absorption (see Goossens et al. 2011 for a review of this damping mechanism). In agreement with observation, theoretically it was predicted that this particular process causes coronal waveguides, such as loops, to act as natural low-pass filters for kink waves (Terradas et al. 2010). In this Letter, for the first time, we study the frequency-filtering properties of chromospheric flux tubes for the particular case of broadband frequency torsional Alfvén waves driven by a realistic photospheric vortex motion. This is motivated by the range of frequencies of these waves detected by Jess et al. (2009), which had the strongest power between 2 and 3 mHz.

Observed vortex motions in the lower atmosphere due to convection (see, e.g., Bonet et al. 2008) generate a wide variety of MHD wave modes (Fedun et al. 2011a, 2011b), and due to their inherent shearing motions are the most likely drivers of the torsional Alfvén waves detected by Jess et al. (2009). In the eigenmode study by Verth et al. (2010a), they proposed that torsional Alfvén waves were the ideal waves to probe the *radial* structure of chromospheric flux tubes since these waves can exist independently on magnetic surfaces. Here we explore this idea further by numerically modeling a vortex driver at the footpoint of an open magnetic flux tube.

2. NUMERICAL SETUP OF THE PROBLEM

We have used the innovative Sheffield Advanced Code (SAC) to carry out our modeling (see Shelyag et al. 2008 for details). To perform the 3D numerical simulation in realistic lower solar atmosphere, i.e., the photospheric and chromospheric regions, the VAL IIIC atmosphere model (Vernazza et al. 1981) has been used as a background. The computational box is 2 Mm wide in x and y directions and 1.6 Mm high in the vertical z direction, with a resolution of $100 \times 100 \times 196$ grid points, respectively. The open magnetic flux tube, modeled as an axially symmetric magnetic field configuration, is obtained analytically and based on a self-similar approach (see Schlüter & Temesváry 1958; Deinzer 1965; Cameron et al. 2008; Shelyag et al. 2009; Fedun et al. 2011a, 2011b). The flux tube footpoint magnetic field strength is around 1000 G (at the center of the tube) and decreases to a few tens of Gauss at the top boundary of the computational domain ($z = 1.6$ Mm, i.e., still within the chromospheric region). Recently, Jess et al. (2010) have reported measured values of photospheric magnetic bright point (MBP) magnetic field, i.e., at the footpoint of our simulated magnetic flux tube, to be of kilogauss strength. The flux tube footpoint radius R is 0.1 Mm. The magnetohydrostatic equilibrium is governed by the following equation:

$$-(\mathbf{B}\cdot\nabla)\,\mathbf{B} + \nabla\left(\frac{\mathbf{B}^2}{2}\right) + \nabla p = \rho\mathbf{g}, \qquad (1)$$

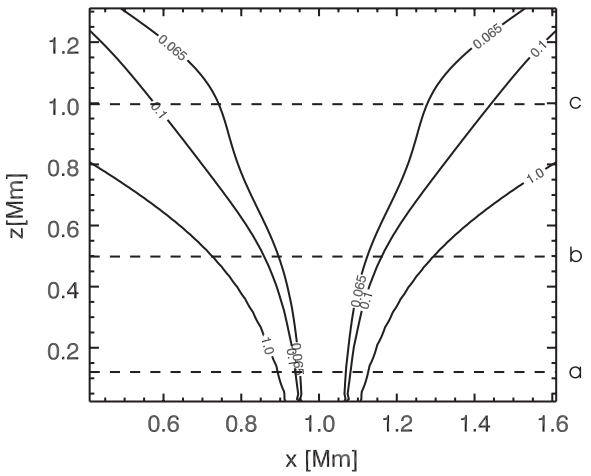

Figure 1. Two-dimensional vertical cross-cut of our simulated magnetic flux tube in terms of plasma-β values at the center of the computational domain. The horizontal dashed lines at (a) 0.12 Mm, (b) 0.5 Mm, and (c) 1.0 Mm correspond to the levels of the horizontal 2D cross-cuts where the maximum power frequency has been taken (see Figure 4).

where $\mathbf{B}$ is the background magnetic field, p is the background kinetic pressure, g is the solar gravitational acceleration, and ρ is the background density. Note that the magnetic field strength is normalized by the factor $\sqrt{\mu_0}$, where μ_0 is the magnetic permeability. The density and gas pressure deviations are calculated from their non-magnetic equilibrium counterparts by using the magnetostatic force balance accordingly to Equation (1). In the radial direction, the ratio of the full width at half-maximum (FWHM) of the simulated open magnetic flux tube at height 0.5 Mm to the FWHM at height 1.2 Mm is 2.5. Therefore, the geometric expansion of our flux tube model agrees well with the indirect observational measurements of the FWHM of a chromospheric magnetic flux tube recently reported by, e.g., Kontar et al. (2008, see their Figure 5).

The structure of the constructed open magnetic flux tube in terms of plasma-β is shown in Figure 1. Due to the realistic simulated strength of the magnetic field at the photospheric/chromospheric region the plasma-β at the central region of the magnetic flux tube is less than one at any height. Similar magnetic configurations, but constructed by different numerical methods, have been used by, e.g., Bogdan et al. (2003), Hasan et al. (2005), and others.

The vortex driver mimicking observed swirls (see Pötzi & Brandt 2005; Bonet et al. 2008, 2010; Wedemeyer-Böhm & Rouppe van der Voort 2009; Steiner et al. 2010) has been applied to excite MHD waves in a realistically simulated lower solar atmosphere. Bonet et al. (2008) have reported that the mean lifetime of observed circular motions turns out to be $t = 5.1 \pm 2.1$ minutes. Accordingly with these estimates, the temporal behavior of the simulated torsional driver is defined as a superposition of discrete frequencies, ranging from $\omega = 2.8$ to 8.3 mHz. These frequencies correspond to time periods 2–6 minutes. Spatially, in the horizontal plane the source is centered at the magnetic flux tube axis and in the vertical direction is located just under the height corresponding to the solar temperature minimum. The amplitude of the driver is 200 m s^{-1}. Similar vortex structures in the photosphere have been studied by direct numerical HD/MHD convection simulations by, e.g., Stein & Nordlund (1998), Kitiashvili et al. (2011), and Shelyag et al. (2011a, 2011b). Analytically the

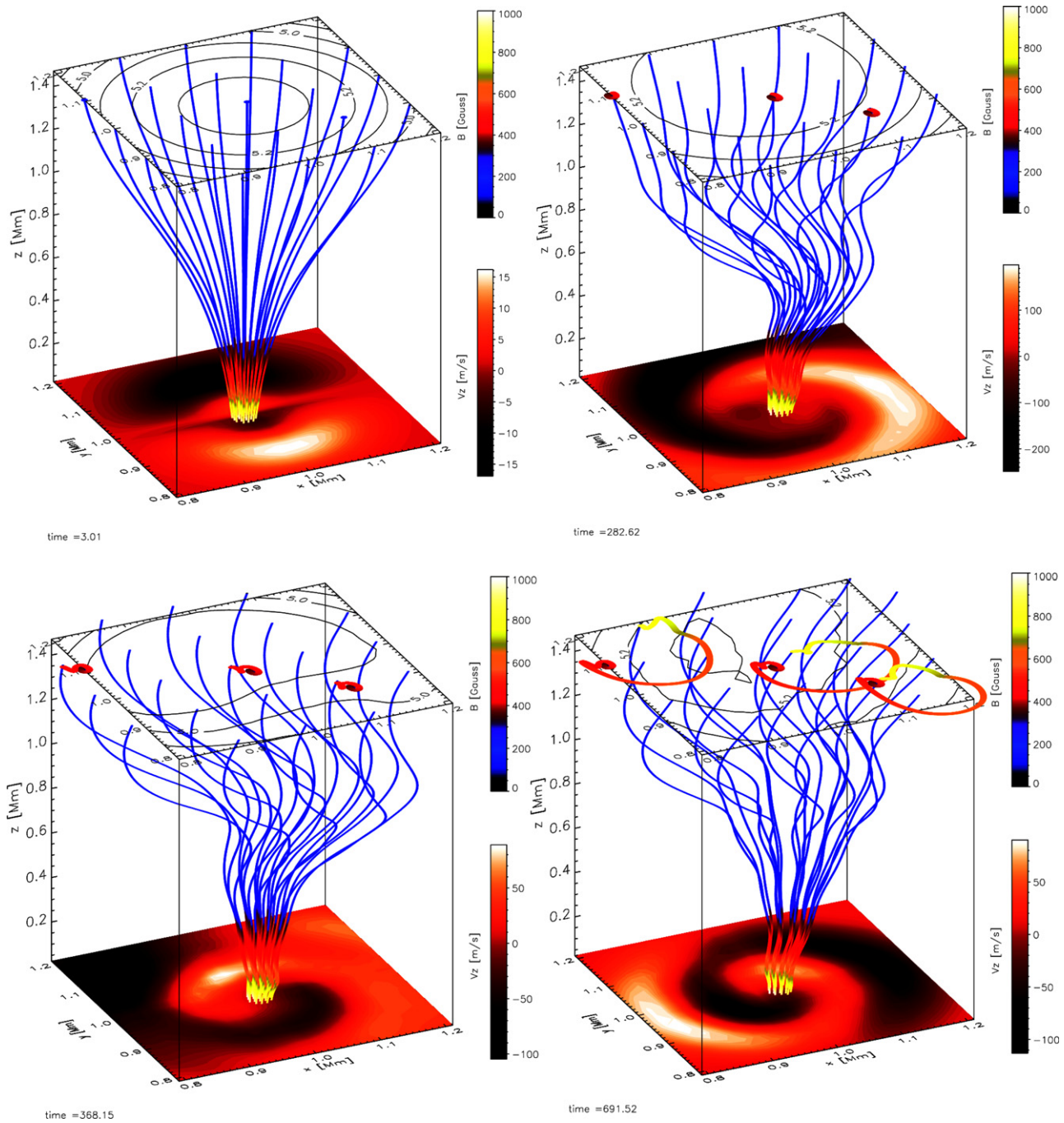

Figure 2. Three-dimensional snapshots of the MHD wave propagation in an open magnetic flux tube are shown. The thin multicolor curves represent the magnetic field lines. The lower and upper color bars correspond to the vertical velocity V_z at the level of the driver location and to the strength value of the magnetic field along the magnetic field lines, respectively. The black iso-contours of the magnetic field labeled by appropriate value of the strength of the magnetic field are shown in the top horizontal slice taken at height $h = 1.4$ Mm. At the bottom of each snapshot the horizontal cross-cut at the location of the swirl driver is shown. The 3D trajectory of the top ends of the three representative magnetic field lines are shown as colored thick curves.

(A color version of this figure is available in the online journal.)

velocity perturbation components V_x and V_y of the implemented driver are described as

$$V_x = A_0 N e^{-\frac{(r-r_0)^2}{\Delta r^2}} e^{-\frac{(z-z_0)^2}{\Delta z^2}} \sum_{i=0,4} \sin\left(\frac{2\pi t}{T_i}\right),$$

$$V_y = A_0 N e^{-\frac{(r-r_0)^2}{\Delta r^2}} e^{-\frac{(z-z_0)^2}{\Delta z^2}} \sum_{i=0,4} \cos\left(\frac{2\pi t}{T_i}\right),$$

where A_0 is the amplitude of the initial perturbation; N is the normalization coefficient; $\Delta r = 0.1$ Mm and $\Delta z = 0.01$ Mm are the half-width of the Gaussian spatial profiles of the driver in the radial and vertical directions, respectively; driver period values are $T_0 = 120$ s, $T_1 = 180$ s, $T_2 = 240$ s, $T_3 = 300$ s, and $T_4 = 350$ s; and $r = \sqrt{x^2 + y^2}$ is the radial distance.

Each component of the simulated driver is fixed to have the same amplitude, because we primarily want to investigate the frequency-filtering properties of the magnetic flux tube, i.e.,

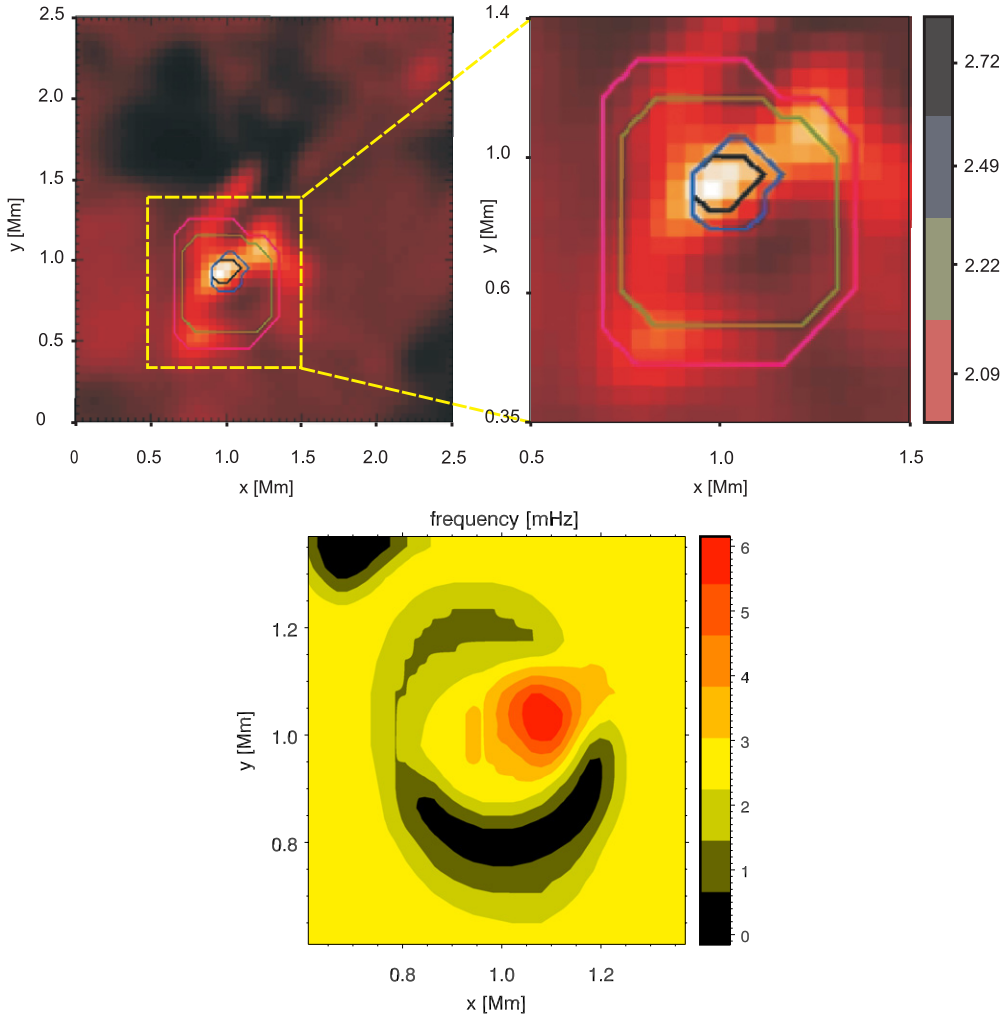

Figure 3. Observational FWHM power frequency of Hα distribution of the photospheric magnetic bright point (top panel and zoom in) and the frequency map across the computational domain obtained numerically (bottom panel).

(A color version of this figure is available in the online journal.)

distribution of frequency power inside the tube due to generated waves. A similar driver, but with only a single frequency, $\omega = 33.3$ mHz, has been used in Fedun et al. (2011b).

3. NUMERICAL SIMULATION AND ANALYSIS

Snapshots of the magnetic field distribution and evolution in the computational box are shown in Figure 2. Each traced magnetic field line has a color scale corresponding to the strength of the magnetic field. At the base of the numerical box, the x–y horizontal cross-cut at the location of the driver is shown. The iso-contours of the magnetic field are shown with a horizontal slice at height $h = 1.4$ Mm. Also, three sample trajectories of magnetic field lines are depicted as thick color curves at the top region of the numerical box. Note that the darker color of the trajectory corresponds to the earlier simulation time and the lighter color to the later. At the upper left panel of Figure 2, we have plotted the initial configuration of the magnetic field. Next, the panels represent a rich pattern of propagating MHD waves and varying tube shape at times $t \sim 283$, 368, and 692 s, respectively.

It is predictable that such a complex photospheric driver will generate a broadband frequency range of MHD waves, i.e., fast/slow magnetoacoustic and (torsional) Alfvén waves. In this Letter, we focused only on the torsional Alfvén component of the generated waves. The torsional Alfvén wave in a 3D geometry is an independent azimuthal motion within separate magnetic surfaces in a flux tube. In cylindrical coordinates (r, ϕ, z), this means that the V_ϕ components of velocity can have different amplitudes and frequencies within each surface. To analyze the dynamic behavior within these surfaces, we have Fourier decomposed the two-dimensional (2D) time–distance diagrams of the azimuthal (V_ϕ) component of velocity at different heights across the flux tube. The bottom panel of Figure 3 demonstrates the spatial distribution of the Fourier transformed maximum power frequency at height 0.5 Mm of torsional Alfvén waves generated by simulated broadband vortex photospheric motion. For comparison, in the top panel we have plotted the FWHM power frequency map of Hα from the data set of Jess et al. (2009). The observed iso-contours of maximum power frequency are overplotted on an image of the underlying solar photospheric magnetic bright point. Note the strong similarities between the observed and simulated maximum power frequency map.

Previously, Verth et al. (2010a) analytically investigated standing torsional Alfvén waves in self-similar finite width 2D axisymmetric flux tubes and found that the radial eigen-frequency distribution showed a strong correspondence to the

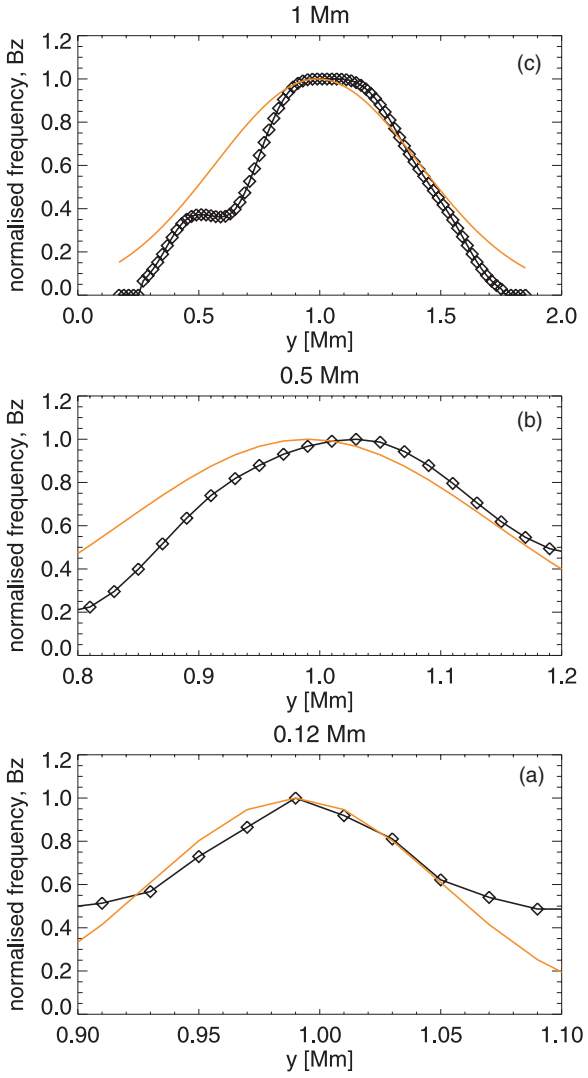

Figure 4. Normalized maximum power frequency as a function of horizontal distance at height (black curve) (a) 0.12 Mm, (b) 0.5 Mm, and (c) 1.0 Mm, i.e., across the magnetic flux tube, inside the plasma-$\beta = 1$ contour (see Figure 1). The overplotted normalized background magnetic field strength is shown as the solid orange curve.

(A color version of this figure is available in the online journal.)

magnetic field strength. From our simulations of realistically driven propagating torsional Alfvén waves, we now report the discovery of natural frequency filtering that can be exploited to give an insight into the chromospheric magnetic field strength distribution. Importantly for chromospheric magnetoseismology, the spatial distribution of the normalized magnetic field at different heights 0.12 Mm, 0.5 Mm, and 1.0 Mm compared with the normalized maximum power frequency at the same horizontal cross-cuts have very similar profiles (see Figure 4). Small horizontal shifts of the maximum power frequency distribution with respect to the background magnetic field strength (see, e.g., Figure 4(b)) can be explained by the presence of other non-Alfvénic wave motions in the analyzed V_ϕ velocity component or by global motion, i.e., due to complex swaying and vortical fluid motion caused by the realistic driver. It is also important to note that the analyzed V_ϕ velocity component is only an approximation of the purely tangential component of velocity within magnetic surfaces. However, our simulations show that the magnetic flux tube's frequency-filtering properties are a robust mechanism for determining its radial magnetic structure. This suggests that the observed maximum power frequency map of the type shown in the top panel of Figure 3 could indicate the chromospheric magnetic field strength distribution above the observed bright point. If we could construct a similar data set, but with maximum power frequency maps at various different heights in the chromosphere, this may allow us to construct a 3D magnetic map of the chromosphere above such bright points.

4. CONCLUSION

Since the torsional Alfvén waves can be generated independently on each magnetic surface, we can resolve the frequency power as a function of radius in the model chromospheric flux tube. At fixed heights in our model chromosphere we constructed a maximum power Fourier frequency map that shows the spatial distribution of the wave power. It is found that the center of the flux tube acts as a natural high-pass filter for propagating torsional Alfvén waves. When normalized peak frequency power and magnetic field strength are compared as a function of flux tube radius, they exhibit an almost one-to-one correspondence (see Figure 4). A maximum power Fourier frequency map of propagating torsional Alfvén waves produced in Hα using spectroscopic data from the Swedish Solar Telescope (Jess et al. 2009) exhibits a similar spatial frequency peak power distribution. This suggests a real possibility of exploiting torsional Alfvén waves to reconstruct the magnetic field in x, y, and z directions at the chromospheric height of the Sun's atmosphere.

R.E. acknowledges M. Kéray for patient encouragement and is grateful to NSF, Hungary (OTKA, Ref. No. K83133).

REFERENCES

Banerjee, D., Erdélyi, R., Oliver, R., & O'Shea, E. 2007, Sol. Phys., 246, 3
Bogdan, T. J., Carlsson, M., Hansteen, V. H., et al. 2003, ApJ, 599, 626
Bonet, J. A., Márquez, I., Sánchez Almeida, J., Cabello, I., & Domingo, V. 2008, ApJ, 687, L131
Bonet, J. A., Márquez, I., Sánchez Almeida, J., et al. 2010, ApJ, 723, L139
Cameron, R., Gizon, L., & Duvall, T. L., Jr. 2008, Sol. Phys., 251, 291
Centeno, R., Trujillo Bueno, J., & Asensio Ramos, A. 2010, ApJ, 708, 1579
Deinzer, W. 1965, ApJ, 141, 548
Fedun, V., Shelyag, S., & Erdélyi, R. 2011a, ApJ, 727, 17
Fedun, V., Shelyag, S., Verth, G., Mathioudakis, M., & Erdélyi, R. 2011b, Ann. Geophys., 29, 1029
Gabriel, A. H. 1976, Phil. Trans. R. Soc. A, 281, 339
Goossens, M., Erdélyi, R., & Ruderman, M. S. 2011, Space Sci. Rev., 158, 289
Hasan, S. S., van Ballegooijen, A. A., Kalkofen, W., & Steiner, O. 2005, ApJ, 631, 1270
He, J.-S., Marsch, E., Tu, C.-Y., & Tian, H. 2009, ApJ, 705, L217
Jess, D. B., Mathioudakis, M., Christian, D. J., Crockett, P. J., & Keenan, F. P. 2010, ApJ, 719, L134
Jess, D. B., Mathioudakis, M., Erdélyi, R., et al. 2009, Science, 323, 1582
Judge, P. G. 2009, A&A, 493, 1121
Kitiashvili, I. N., Kosovichev, A. G., Mansour, N. N., & Wray, A. A. 2011, ApJ, 727, L50
Kontar, E. P., Hannah, I. G., & MacKinnon, A. L. 2008, A&A, 489, L57
Lagg, A. 2007, Adv. Space Res., 39, 1734
Metcalf, T. R., Jiao, L., McClymont, A. N., Canfield, R. C., & Uitenbroek, H. 1995, ApJ, 439, 474
Morton, R. J., Erdélyi, R., Jess, D. B., & Mathioudakis, M. 2011, ApJ, 729, L18
Pötzi, W., & Brandt, P. N. 2005, Hvar Obs. Bull., 29, 61
Schlüter, A., & Temesváry, S. 1958, in IAU Symp. 26, Electromagnetic Phenomena in Cosmical Physics, ed. B. Lehnert (Cambridge: Cambridge Univ. Press), 263
Shelyag, S., Fedun, V., & Erdélyi, R. 2008, A&A, 486, 655
Shelyag, S., Fedun, V., Keenan, F. P., Erdélyi, R., & Mathioudakis, M. 2011a, Ann. Geophys., 29, 883
Shelyag, S., Keys, P., Mathioudakis, M., & Keenan, F. P. 2011b, A&A, 526, A5

Shelyag, S., Zharkov, S., Fedun, V., Erdélyi, R., & Thompson, M. J. 2009, A&A, 501, 735
Solanki, S. K., Lagg, A., Woch, J., Krupp, N., & Collados, M. 2003, Nature, 425, 692
Stein, R. F., & Nordlund, A. 1998, ApJ, 499, 914
Steiner, O., Franz, M., Bello González, N., et al. 2010, ApJ, 723, L180
Taroyan, Y., & Erdélyi, R. 2009, Space Sci. Rev., 149, 229
Terradas, J., Goossens, M., & Verth, G. 2010, A&A, 524, 23
Tsuneta, S., Ichimoto, K., Katsukawa, Y., et al. 2008, ApJ, 688, 1374
Vernazza, J. E., Avrett, E. H., & Loeser, R. 1981, ApJS, 45, 635
Verth, G., Erdélyi, R., & Goossens, M. 2010a, ApJ, 714, 1637
Verth, G., Goossens, M., & He, J.-S. 2011, ApJ, 733, L15
Verth, G., Terradas, J., & Goossens, M. 2010b, ApJ, 718, L102
Wedemeyer-Böhm, S., & Rouppe van der Voort, L. 2009, A&A, 507, L9
Zaqarashvili, T. V., & Erdélyi, R. 2009, Space Sci. Rev., 149, 355
Zhang, H., & Zhang, M. 2000, Sol. Phys., 196, 269